Computers in Biology and Medicine 174 (2024) 108450

Contents lists available at ScienceDirect

Computers in Biology and Medicine

journal homepage: www.elsevier.com/locate/compbiomed

New non-local mean methods for MRI denoising based on global self-similarity between values

Shiao Li [a], Fei Wang [b], Song Gao [a,*]

[a] Institute of Medical Technology, Peking University Health Science Center, Haidian District College Road No. 38, 100191, Beijing, China
[b] Key Laboratory of Carcinogenesis and Translational Research, Department of Radiation Oncology, Beijing Cancer Hospital, Haidian District Fucheng Road No. 52, 100142, Beijing, China

ARTICLE INFO

Keywords:
MRI
Denoising
NLM
PRI-NL-PCA
PNLM-PCA
Self-similarity

ABSTRACT

Magnetic resonance imaging (MRI) is a non-invasive medical imaging technique that provides high-resolution 3D images and valuable insights into human tissue conditions. Even at present, the refinement of denoising methods for MRI remains a crucial concern for improving the quality of the images. This study aims to improve the prefiltered rotationally invariant non-local principal component analysis (PRI-NL-PCA) algorithm. We relaxed the original restrictions using particle swarm optimization to determine optimal parameters for the PCA part of the original algorithm. In addition, we adjusted the prefiltered rotationally invariant non-local mean (PRI-NLM) part by traversing the signal intensities of voxels instead of their spatial positions to reduce duplicate calculations and expand the search volume to the whole image when estimating voxels' signal intensities. The new method demonstrated superior denoising performance compared to the original approach. Moreover, in most cases, the new algorithm ran faster. Furthermore, our proposed method can also be applied to process Gaussian noise in natural images and has the potential to enhance other NLM-based denoising algorithms.

1. Introduction

Magnetic resonance imaging is a valuable tool for visualizing the three-dimensional structure and internal characteristics of human tissues and organs. It offers non-invasive insights into a wealth of physiological and pathological information, playing a crucial role in both clinical diagnosis and scientific research [1]. Currently, MRI stands as one of the most prevalent techniques in clinical medical imaging. However, inherent noise during the image acquisition process can introduce errors that may impact the accurate interpretation of diseases. Consequently, denoising medical images becomes an essential pre-processing step in disease diagnosis [2].

Principal component analysis (PCA) is commonly employed for dimensionality reduction, but PCA can also be used for denoising. The essence of PCA denoising is maximum separability, where the signal and noise are effectively separated by the orthogonal linear transformation. When applying PCA decomposition to the image, it is observed that the signal-related components tend to be concentrated in a limited subset of principal components, while the noise is evenly dispersed across all components. The eigenvectors corresponding to small eigenvalues are often associated with noise, and by discarding them, a certain degree of denoising is achieved. The adaptive version of PCA was initially proposed by Muresan and Parks [3]. In their work, PCA decomposition was performed on a localized group of image patches. Subsequently, the algorithm was improved: similar patches were grouped before PCA decomposition was performed, and the process was iterated to more effectively minimize noise [4]. Additionally, Bao et al. [5] and Lam et al. [6] introduced PCA-based denoising methods for diffusion weighted imaging (DWI).

The non-local mean (NLM) method achieves remarkable performance based on the similarity between each two patches in the image. At its core, the NLM method relies on weighted averaging, which takes advantage of the high degree of redundancy in patch similarity. NLM believes that all natural images contain excess information, and for each voxel in the image, there exist other voxels that are similar to it but may not be located in its spatial neighbor region. Several different versions of the NLM algorithms have been developed to date. These NLM algorithms not only preserve edges but also enhance the signal-to-noise ratio and computational efficiency. Importantly, NLM operates independently of any specific image model assumption. Its origins can be traced back to the work of Buades et al. [7], in which the idea of NLM and its corresponding algorithm was proposed for the first time. NLM, used initially to denoise natural images, was developed

* Corresponding author.
E-mail addresses: ShiaoLi@stu.pku.edu.cn (S. Li), fei.wang1225@outlook.com (F. Wang), gaoss@bjmu.edu.cn (S. Gao).

https://doi.org/10.1016/j.compbiomed.2024.108450
Received 27 August 2023; Received in revised form 20 March 2024; Accepted 7 April 2024
Available online 9 April 2024

further to denoise MR images [8]. Continual refinement has led to reduced computational overhead [9], along with rotational invariance and integration with other denoising algorithms [10,11]. Refer to Bhujle and Vadavadagi [2] for a comprehensive review of modern NLM algorithms.

Metaheuristic algorithms (MAs) have gained significant popularity across various applied fields in recent years. This may be due to their remarkable performance and efficiency in solving optimization problems using fewer computational resources and time compared to deterministic algorithms [12]. Specifically, MAs excel at tackling complex problems within a reasonable time by avoiding entrapment in local optima and prioritizing simplicity, thereby providing satisfactory solutions [13,14]. Among MAs, Monarch Butterfly Optimization [15], weIghted meaN oF vectOrs [16], Harris Hawks Optimization [17], Particle Swarm Optimization [18] are widely used. MAs are nothing more than exploration and exploitation. The former demonstrates the richness of randomness and adaptability, while the latter emphasizes the local search capability based on prior explorations.

In the study of Bhujle and Vadavadagi [2], the authors compared several NLM algorithms for denoising Ricianly perturbed images and found that PRI-NLM3D [10] had the best performance in processing Ricianly perturbed MR images obtained from a single coil. The PRI-NL-PCA algorithm, proposed by Manjón et al. [11] is similar to the PRI-NLM3D, but its guide images are obtained by a different prefilter. Meanwhile, the PRI-NL-PCA filter has better denoising performance than PRI-NLM3D. Recent proposed deep learning methods, such as the multichannel version of denoising convolutional neural networks (MCDnCNN) [19] and residual encoder–decoder Wasserstein generative adversarial network (RED-WGAN) [1], have better denoising performance than many traditional denoising methods. However, these deep learning approaches require a large number of high-quality images for the training set. This paper aims to improve the PRI-NL-PCA algorithm further. In this article, to improve efficiency and for convenience, we first used the built-in function of MATLAB to implement the particle swarm optimization algorithm to find the optimal parameter group for the PCA part of the algorithm. Then, we proposed a new NLM structure that traversed values instead of coordinates. This approach reduces redundant calculations and expands the search range for estimating voxel signal intensity. By discarding some unimportant calculations and using mathematical principles to randomly and uniformly sample the entire image, the algorithm achieves improved efficiency. The primary contribution of this article is that, under the same noise level, the proposed PCA prefiltered non-local mean (PNLM-PCA) algorithm not only exhibits higher Peak Signal-to-Noise Ratio (PSNR) and Structural Similarity Index (SSIM) compared to PRI-NL-PCA, and demonstrates faster performance in most scenarios. To the best of our knowledge, this paper pioneers the concept of value-based traversal in NLM-based denoising algorithms, leading to enhanced noise reduction in magnetic resonance images.

The paper is organized as follows. The methods are described in Section 2. The experiments and main results are given in Section 3. In Section 4, the findings are discussed, and conclusions are made.

2. Methods

A denoising problem is usually defined as follows: Given a noisy image Y, treat it as the sum of the original noise-free image Z and some noise n:

$$Y = Z + n \tag{1}$$

Thus, for any denoising algorithm, the goal is to find a good estimate $\hat{Z}$ for a given noisy image. Researchers usually use metrics such as the PSNR and the SSIM to evaluate how good an estimate is.

2.1. PRI-NL-PCA method

2.1.1. Principle component analysis

This method only looks for similar sets of patches in a search window. In a 3D window, for each 3D patch, this method selects a set of (M-1) patches in the window that are the most similar to it and transforms those M patches into row vectors to form a sample matrix X. The values of the elements of the row vectors reflect the signal intensity. The similarity between two patches is measured by the Euclidean distance between their corresponding vectors. X is a matrix of $d^3 \times M$, where d denotes the number of voxels contained in one edge of a cubic patch. The sample matrix is centralized to find its covariance matrix and further to find the covariance matrix's eigenvalues and eigenvectors. Eigenvectors whose eigenvalues are less than $\tau\sigma$ are discarded, and σ is calculated using the following equations:

$$\hat{\sigma} = \beta\sqrt{median\left(\lambda_s\right)}\ ,\ \lambda_s = \left\{\lambda_j \middle| \sqrt{\lambda_j} \leqslant T median\left(\sqrt{\lambda}\right)\right\} \tag{2}$$

where T is used to differentiate between characteristic values that represent signals and those that represent noise. λ_s is a short truncated version of the original eigenvalue array. τ is a threshold parameter. The eigenvalues of the covariance matrix represent the magnitude of the variance of the data in the direction of the principal components. The remaining eigenvectors corresponding to the larger eigenvalues form a projection matrix W^*. $W^*(W^*)^T$ is multiplied by the centralized sample matrix, and the result obtained after decentralization is the desired denoising matrix. Considering that each voxel is contained in more than one patch, estimates of the signal intensity and standard deviations for a voxel is combined by the uniform averaging rule.

In the resulting image obtained through PCA denoising of the magnitude image, the signal intensity value for each voxel is determined by the uniform average of patches that contain the voxel. This method is similar to obtaining the first moment of the Rician distribution. However, according to Koay and Basser [20], the first moment is biased and is not equivalent to the true signal intensity without noise. In the presence of Rician noise, the first and second moments of the signal intensity can be expressed analytically by the equations

$$\langle u\rangle_{p_r} = \sqrt{\frac{\pi}{2}}\sigma_g e^{-\frac{v^2}{4\sigma_g^2}}\left[\left(1+\frac{v^2}{2\sigma_g^2}\right)I_0\left(\frac{v^2}{4\sigma_g^2}\right)+\frac{v^2}{2\sigma_g^2}I_1\left(\frac{v^2}{4\sigma_g^2}\right)\right] \tag{3}$$

and

$$\left\langle u^2\right\rangle_{p_r} = 2\sigma_g^2 + v^2 \tag{4}$$

where σ_g is the Gaussian noise's standard deviation present in both the real and imaginary images, p_r represents Rician distribution, I_0 and I_1 denote the zeroth and the first kind modified Bessel functions respectively. v is the original signal intensity, and u is the measured signal intensity. The formula (3) and a pre-calculated look-up table must be utilized to transform the biased estimation into an unbiased one.

2.1.2. Prefiltered rotationally invariant non-local mean filter

For the traditional NLM estimator, the restored value of a certain voxel's signal intensity is the linear weighted average of the intensity of each voxel in a certain region of the image:

$$\hat{v}(i) = \frac{\sum_{j\in\Omega} w(i,j)\,u(j)}{\sum_{j\in\Omega} w(i,j)} \tag{5}$$

The meanings of u and v have been mentioned earlier. Ω is the search volume around voxel i. Weight w(i, j) is allocated to u (j) when restoring voxel i.

The result may be susceptible to noise if similar patches are searched from noisy images. The original image without noise can be used to measure the similarity between two patches more accurately. However, researchers often do not have such a perfect image in practice, so it is necessary to take a pre-denoised image as a guide instead.

$$w(i,j) = \begin{cases} \exp\left[-\frac{1}{2}\left(\frac{(g(i)-g(j))^2+3\left(\mu_{Ni}-\mu_{Nj}\right)^2}{2h_i^2}\right)\right] & if\ \left|\mu_{Ni}-\mu_{Nj}\right| < h_i \\ 0 & otherwise \end{cases} \tag{6}$$

In the formula (6), g denotes the signal intensity of the guide image. The averages of the patches N_i and N_j surrounding voxel i and j in the guide image are represented by μ_{Ni} and μ_{Nj}. h_i is correlated with the standard deviation of the noise in voxel i, h_i=0.4σ_g, as mentioned in Manjón et al. [11]. The weights here are not yet normalized and should be calculated by multiplying them by the normalization factor to ensure that the sum of the weights corresponding to all voxels j in the search volume of voxel i is 1.

Meanwhile, utilizing the guide map to space-weight the original noisy MR image by (5) results in a biased estimate due to the Rician distribution. The second-moment formula of the Rician distribution is used to construct the following unbiased estimator:

$$\hat{v}(i) = \sqrt{\max\left(\left(\frac{\sum_{j\in\Omega} w(i,j)\,u^2(j)}{\sum_{j\in\Omega} w(i,j)}\right) - 2\sigma_g^2(i)\ ,0\right)} \tag{7}$$

2.2. The particle swarm optimization method (PSO)

We first adjusted the trimmed median method in Manjón et al. [11] to the form of (2) in an attempt to overcome the original subjective shortcomings. This paper also tried to relax the restriction of M=d^3 and explore the set of parameters that can optimize the performance of the NL-PCA filter. The effects of d, M, w, T, and $\tau\beta$ on algorithm performance were considered, where M is the number of similar patches in a group, w denotes the radius of a search window($(2w+1)^3$ voxels lies in it), $\tau\beta$ and T are threshold parameters mentioned in Section 2.1. Considering the numerous parameters to be optimized, traversing all possible cases would be very time-consuming, we decided to use a meta-heuristics algorithm to find the parameter set that maximizes the performance of NL-PCA.

This paper split the original 3D image into closely spaced 3D windows of equal size since searching the entire volume with highly overlapped windows will be time-consuming and not worth it when running the PSO algorithm in this work. Considering that the original 3D image may not be divisible by the size of the 3D window, after the final element in each dimension, the mirror reflection elements of the corresponding array are padded along the boundaries using the padarray function in MATLAB.

The small eigenvalues of the covariance matrix of the sample obtained by the PCA method are often related to noise, and the denoising can be realized to a certain extent by discarding their corresponding eigenvectors. A reasonable setting of $\tau\beta$ values can effectively remove noise components. To better define the noise part and the signal part, it is necessary to set the T value appropriately. Manjón et al. [11] subjectively fixed $T = 2$ in Eq. (2) based on an example of PCA eigenvalues. In this article, T was a parameter that needed to be optimized. The parameter β was used in Manjón et al. [11] to obtain the noise map, while in this study, it was multiplied with the parameter τ as a whole to remove small eigenvalues. Another weakness of Manjón et al. [11] in the analysis is that the constraint M =d^3 does not necessarily make the PSNR reach the optimal value, and there is no theoretical basis to prove it.

For the PSO algorithm, this paper set SwarmSize to 50, maxIterations to 50, FunctionTolerance to 1e-3, and adopted the default values of MATLAB for the rest. 1% Gaussian noise was added to the ground truth, and the PSO algorithm was run to obtain the set of optimal parameters (d, M, w, $\tau\beta$, T) when the PSNR reached the maximum.

When the particle swarm optimization algorithm was used, to improve the search efficiency, we made the following qualification:

$$\begin{cases} 2 \leqslant d \leqslant w+1 \\ d^3 \leqslant M \leqslant (2w+2-d)^3 \\ 2 \leqslant w \leqslant 3 \end{cases} \tag{8}$$

The meanings of d, M, $\tau\beta$, and T have been mentioned above. M=$(2w + 2 - d)^3$ corresponds to the situation in which all patches in the search window are selected to form a group. This paper initially allowed the upper limit of w to be 4, but later found this unnecessary. This is because it greatly increased the running time of the particle swarm optimization algorithm and did not necessarily help the denoising performance of the NL-PCA algorithm compete with those of the state-of-the-art methods. It also does not affect the final contributions of our paper. When the number of samples is smaller than the data dimension in the sample matrix, the effect of PCA will be limited. This is caused by the singularity of the covariance matrix, which will cause the eigenvalues of part of the eigenvectors to become 0. According to the experiment, in this case, the smaller the number of samples, the more eigenvalues of the covariance matrix will be 0, the lower the threshold, and the image will hardly be denoised at last. For a better denoising effect, more samples need to be added to restore the covariance matrix to full rank. The above discussion explains the constraint $M \geqslant d^3$. $d \leqslant w+1$ because the left side of the inequality in the second line of (8) must be smaller than the right side. $M \leqslant (2w+2-d)^3$ because the number of similar patches selected in a 3D window cannot exceed the total number of patches in the window.

2.3. A new NLM method based on self-similarity value by value

This article proposed to adjust the structure of PRI-NLM by traversing values instead of coordinates, in order to improve the algorithm. At this point, the search volume in the formula (7) is the entire image. PRI-NLM filter in Manjón et al. [11] uses the voxel signal intensity in a small search volume of the image to determine the signal intensity of the central voxel of that volume. The setting of the size of the search volume fully considers the computational complexity and the quality of the results. However, a search window still cannot replace the entire image, and this method also imposes limitations $\left|\mu_{Ni} - \mu_{Nj}\right| < h_i$ to further improve the calculation speed, as shown in (6). Upon careful analysis of the formula (6), we will find that g and μ have a more direct impact on the weight values. Voxels at different positions in the image may have similar (g, μ) values. According to NLM, the contribution of these voxels to the estimated signal intensity of a certain voxel in the image should also be similar, i.e., $w(i,j) = \tilde{w}(\Delta g, \Delta\mu)$. Among them, $\Delta g = |g(i) - g(j)|$ and $\Delta\mu = \left|\mu_{Ni} - \mu_{Nj}\right|$. Traversing voxels one by one will inevitably result in a lot of repeated calculations. The number of voxels in an MRI image is often as much as 10^6 to 10^7, but the final grayscale value range shown is generally only 0–255, and the values are discrete.

We will now elaborate on the core idea of the new NLM method. The algorithm first requires the input of a guide image and a local mean image. This article abbreviates these two three-dimensional matrices as G and M. M is a three-dimensional matrix composed of local mean values at each voxel in G. Formula (6) can be regarded as a function of two variables, as its value only depends on g and μ at voxel i, while the signal intensity of the guide image and the original noise image remain unchanged. To enhance the effectiveness of PRI-NLM and extend the search scope globally, it is intuitive to consider employing the MATLAB matrix approach. G and M are treated as independent variables of the function. Applying this function can generate denoised 3D images. A possible way to achieve this method is to utilize formula (6) to calculate the weight matrix w(g(i), μ(i), G, M) of each voxel i with the same size as the original input image, forming a six-dimensional matrix or a three-dimensional matrix. However, the size of the matrix in each dimension is the square of the size of the original input matrix. Then, the result matrix is compressed using the formula (7). Since an MRI image itself is already large, creating such a matrix would take up more memory than MATLAB can handle, so this method is not feasible. This work chose to achieve the above goals by sacrificing a certain amount of time to save memory through loop traversal. Unlike Manjón et al. [11], we traversed discrete grayscale values instead of voxels' coordinates. We created two additional matrices, Gr and Mr, in the function, which are obtained by rounding G and M, while the original values of G

and M remain unchanged. Similarly, we can consider formula (7) as a function: $\hat{v}(i) = \hat{v}(g(i), \mu(i)) = f(g, \mu)$. It should be noted that in Gr and Mr, when g or μ is fixed, there is a certain limit to the value of another independent variable of f, and there should be no (g, μ) that is not present in the image. This constraint is used to improve the efficiency of the traversal process. In other words, the new algorithm first calculates the function of two variables in formula (7) temporarily. Then, it uses interpolation to process the input three-dimensional matrices G and M and obtain the denoised image as the final output. The function f is determined by G and M.

Considering the changes in the traversal structure of PRI-NLM, the weights of this algorithm need to be changed to the following form:

$$w(i,j) = \begin{cases} \exp\left[-\frac{(g(i)-g(j))^2}{4h_i^2}\right] & if \ \ |g(i)-g(j)|, \left|\mu_{Ni}-\mu_{Nj}\right| < \lambda h_i \\ 0 & otherwise \end{cases} \tag{9}$$

Among them, λ is an undetermined scalar with an initial value of 3. h_i still equals $0.4\sigma_g$. The reason for simultaneously restricting g and μ is that our search area has changed from the 11 × 11 × 11 search volume in Manjón et al. [11] to the global image. From the perspective of the entire image, the central voxel g values of two patches with similar μ may differ significantly, and such patches are not uncommon. The two limits should take the same threshold λh_i and λ=3, which was discovered by experiments. It was found that this configuration strikes a balance between computational complexity and the quality of the outcomes. On the other hand, we discarded $\left(\mu_{Ni}-\mu_{Nj}\right)^2$ in the weight function to further improve the efficiency of the function since we found in the experiment that this term did not contribute significantly to PSNR and SSIM. This may be because we have already considered structural similarity in the constraint conditions, and the search area has become the entire image. Hence, the difference between the g values of two non-local voxels is more important.

As the noise level increases, the smoothing parameter h also increases. When g or μ is constant, the range of values for another independent variable will also expand, inevitably leading to an increase in computational complexity caused by traversal. On the other hand, as the size of MRI images increases, the computational burden also increases accordingly. To further accelerate the operation of the function, we set two relevant parameters, sg and level:

$$sg = \lceil \frac{C_0}{10} \rceil \tag{10}$$

and

$$level = \frac{\sigma_g}{255} \times 100 \tag{11}$$

Among them, C_0 represents the size of the matrix in the third dimension. The 10 in the formula (10) was obtained experimentally, considering both computational complexity and the quality of the results. The size of the other two dimensions or the cube root of the product of the matrix size in three dimensions may also be acceptable, but all the results in this article are based on (10). If researchers want to improve the filter in the future, we can consider it from this perspective. Note that random and uniform sampling from a population that follows a specific distribution results in a probability distribution that theoretically matches the distribution of the population. We can randomly and uniformly sample all voxels j that satisfy the double restriction of (g, μ) for a specific voxel i, and obtain Gs and Ms from G and M, then calculate w(g(i), μ(i), Gs, Ms), where s represents the sample. The sample size is $\frac{1}{sg \times level}$ of the total number of voxels that meet the requirements. Compared to w(g(i), μ(i), G, M), its computational complexity is smaller. In this way, the execution time of the PRI-NLM filter is minimally affected by the size of the MRI image and the noise level.

Finally, in the experiment, we found that the λ that maximizes the denoising performance of the PNLM-PCA algorithm, PSNR and SSIM, decreased as the level increased. The significance of double restriction is not only to improve computational speed but also to improve accuracy. This relationship approximately satisfies linearity:

$$\lambda = 3.2 - 0.3 \times \frac{level + 1}{2} \tag{12}$$

So λ should not be a constant but a variable that changes with the noise level.

2.4. Noise estimation for Rician noise

The estimate of noise affects not only the Rician correction of the PCA-filtered image but also the degree of smoothing of the non-local mean filter and the secondary Rician correction required during weighted averaging. Thus, an accurate noise estimation is crucial in optimizing the denoising performance.

Manjón et al. [11] obtained Gaussian-like local estimates using Eq. (2), and then corrected them Ricianly. However, the noise estimation method mentioned above was not accurate enough at low noise levels.

Coupé et al. [21] proposed an object-based median absolute deviation (MAD) estimator designed for Rician noise. Note that the low sub-band LLL obtained from the 3D wavelet decomposition contains the feature information, while the highest sub-band HHH is mainly composed of coefficients corresponding to noise. The segmentation of the object is done in the LLL sub-band, and the mask obtained is used to extract coefficients y_i corresponding to the object in the HHH sub-bands. When the noise follows the Gaussian distribution, its standard deviation σ can be obtained by the following equation:

$$\hat{\sigma} = \frac{median\left(|y_i|\right)}{0.6745} \tag{13}$$

Under the Rician noise, an additional analytical iterative correction is needed to obtain unbiased estimates as Koay and Basser [20]. For a detailed understanding of the object-based method mentioned above, this paper recommends referring to the original paper by Coupé et al. [21].

This paper uses the method based on (13) to estimate the Rician noise level of clinical data. It is essential to mention that the bias correction techniques (7) discussed in this paper can be used for single coil or SENSE acquired images, but not for GRAPPA acquired images. The experiments in this study would focus on denoising methodology using constant Rician noise in MRI rather than the nature of the noise itself. Therefore, for simplicity, the subsequent experiments only focused on homogeneous noise.

3. Experiments and results

To facilitate the replicability of the experiments conducted, the MATLAB code utilized in our research will be accessible on the website: https://github.com/qizixinge/PNLM-PCA.

3.1. Experimental data description

BrainWeb MRI phantom [22,23] was used in our experiment. The dataset includes brain images of T1w, T2w, and PDw, which can have a Rician noise level from 1% to 15% of the maximum signal intensity. The 3D image has 181 × 217 × 181 voxels. This paper selected images with 1 mm^3 voxel resolution for download. Only spatially isotropic noise distributions were used for the experiments.

The PSNR and the SSIM [24] were used to measure the denoising performance of the algorithm:

$$PSNR = 20\log_{10}\frac{255}{RMSE} \tag{14}$$

and

$$SSIM(u,v) = \frac{\left(2\mu_u\mu_v\right)\left(2\sigma_{uv}+c_2\right)}{\left(\mu_u^2+\mu_v^2+c_1\right)\left(\sigma_u^2+\sigma_v^2+c_2\right)} \tag{15}$$

RMSE represents the root mean square error between the noiseless and filtered images. $c_1 = (k_1 L)^2$ and $c_2 = (k_2 L)^2$, where L denotes the range with a default value of 255, and $k_1 = 0.01$, $k_2 = 0.03$. μ_u and μ_v are the local mean values of noisy image u and ground truth v, σ_{uv} is the covariance of image u and v, σ_u and σ_v denote local standard deviations of u and v. The above six local estimates were completed by each voxel in the $3 \times 3 \times 3$ neighborhood. The global SSIM value is calculated by averaging all local SSIM estimates. Compared to PSNR, SSIM is more in line with our visual characteristics. For clarity, the values of PSNR and SSIM are only evaluated within the region of interest (ROI), i.e., the head tissues, which are obtained by excluding the background region.

3.2. The optimal parameters

The approximate optimal results for the NL-PCA filter by PSO were d = 3, M = 27, w = 3, $\tau\beta = 2.46$, $T = 2.46$. This result meets our expectations and is consistent with the product of τ=2.1 and β=1.16 given in Manjón et al. [11] (where T=∞).

Manjón et al. [11] obtained the optimal parameter of the NL-PCA filter (d, M, w) = (4, 64, 3) with the constraint M=d^3, which exactly satisfies M= $(2w + 2 - d)^3$. Taking into account the mathematical principle of the PCA method, the eigenvalue of the covariance matrix only needed to be calculated once in each search window, which will significantly improve the efficiency of the code. However, when (d, M, w) = (3, 27, 3), for each patch in a window, it is necessary to search for the 26 most similar patches in the other 124 patches. If the number of overlapping voxels between windows is increased, the code running time will grow as a power function. Although (d, M, w) = (4, 64, 3) is not the optimal solution, the denoising performance corresponding to it can be significantly improved by overlapping windows and even exceeds that corresponding to our optimal solution. To improve the efficiency of the NL-PCA filter when (d, M, w) = (3, 27, 3), this research only looks for patches in each window that are most similar to its central patch. This paper lets step=2 between consecutive windows. However, the images obtained in the experiment were even blurrier than the initial noisy images. According to the above phenomena and the mathematical characteristics of the PCA method, it is believed that the key point of the NL-PCA filter is not non-local but the selection of all patches in search windows.

For the parameter group (d, M, w, $\tau\beta$, T) of the NL-PCA filter, the optimal solution of $\tau\beta$ and T is (2.46, 2.46). Compared with (2.2×1.29, 2) in Manjón et al. [11], our NL-PCA filter only slightly improved under low level noise. This result reflects the rationality of the parameters set by Manjón et al. [11]. From the experiments, we found that the NL-PCA filter had a similar performance for different types of images under the two sets of parameters. However, the latter could perform slightly better at higher noise level.

In addition, we also found that when the threshold τ is constant, directly entering the actual standard deviation of noise into the NL-PCA filter produces better denoising quality compared to the denoising quality obtained using the formula (2). The former is needed to obtain PSNR and SSIM that are as good as Manjón et al. [11] at the same noise level. This phenomenon may be due to inconsistencies between the internal implementation of the codes.

Finally, to improve the robustness of NL-PCA denoising results at various noise levels, this study still followed the parameter settings in Manjón et al. [11]. However, this work did not use β and T, but directly input the accurate noise level into the NL-PCA filter.

3.3. Comparison

3.3.1. The necessity of median filter

As mentioned by Manjón et al. [11], the median filter can significantly promote patch selection in the grouping process of NL-PCA denoising, but our experimental results (see Table 1) show that applying a median filter under low-level noise will have a negative effect on the denoising process. Whether using formula (2) or directly inputting the accurate noise level into the NL-PCA filter, the median filter will have a negative effect on the denoising performance of the NL-PCA algorithm at a noise level of 1%–9%. On the one hand, it may be because the medium to high level noise mentioned in Manjón et al. [11] is relative to a larger range of 1%–15% or 1%–27%. The median filter does enhance the homogeneity of patches within the group, providing a sparser representation, but at the same time, the large eigenvalues representing the signal are also reduced. The median filter will make noisy images noisier at low noise level. On the other hand, it may be due to differences in the code implementation.

Table 1
PSNR and SSIM measurement of different methods on PDw images with different noise levels. The first row of data in the table below is the PSNR and the second row is the SSIM. The following tables are similar.

Denoising type	Noise level				
	1%	3%	5%	7%	9%
Without median filter	45.0878	38.3874	35.2285	33.2349	31.6170
	0.9907	0.9583	0.9246	0.8973	0.8704
With a median filter	31.0778	30.4020	29.5152	28.6376	27.7384
	0.9493	0.9091	0.8889	0.8702	0.8536

Based on the experimental results, this research did not use the median filter in the NL-PCA algorithm.

3.3.2. Analysis of denoising effect under different combinations

In this section, we tested and compared our new NLM method with well-established denoising methods, such as the block matching 4D method (BM4D), to evaluate its performance in denoising 3D MR images. The principle of BM4D is very similar to that of PRI-NL-PCA. In the first stage, both require grouping, collaborative filtering, and aggregation, while in the second stage, the pre-denoising results from the first stage are used for matching. For more details about BM4D, see Maggioni et al. [25].

Seven experiments were conducted: only the NL-PCA method was used to denoise images disturbed by Rician noise; the PRI-NL-PCA filter was used; the PCA prefiltered non-local mean method; the PCA prefiltered Wiener-Filtering (2nd stage of BM4D) method; the BM4D algorithm; the Hard-Thresholding (1st stage of BM4D) prefiltered rotationally invariant non-local mean method; the Hard-Thresholding prefiltered non-local mean method. The experimental results are shown in Table 2. By taking into account all noise levels comprehensively, the denoising performance can be obtained in terms of PSNR and SSIM: $NL-PCA < Bw-NL-PCA < BM4D \approx PRI-Bh \approx PNLM-Bh < PRI-NL-PCA < PNLM-PCA$. The denoising speed between different algorithms: $Bw-NL-PCA < PRI-NL-PCA < PNLM-PCA < NL-PCA < BM4D < PRI-Bh < PNLM-Bh$. According to the experimental results, the new algorithm PNLM-PCA proposed in this paper performs better than the original PRI-NL-PCA in terms of the PSNR and SSIM denoising performance, as well as the denoising speed. We can also observe from the relationship between the denoising performance of different filter combinations that there is often no single type of method that can maximize the enhancement of any other algorithm. This phenomenon may be due to the internal parameter settings of the filter algorithm not being adjusted accordingly.

Fig. 1 provides a visual evaluation of the different results for T2w MS lesion brain images corrupted with 9% Rician noise. All of the methods have the ability to reduce noise to different extents. However, the second-row images show that the PNLM-PCA method outperforms BM4D and PRI-NL-PCA in structure preservation. The results indirectly suggest that PNLM-PCA performs better than PRI-NL-PCA and BM4D in reducing noise and produces the most reliable outcomes compared to the reference images.

To further demonstrate the robustness of the proposed PNLM-PCA approach, the PDw normal brain images were also included. The experimental results for PDw normal images are shown in Table 3.

Table 2
PSNR and SSIM measurement of different methods on T2w MS lesion images with different noise levels.

Denoising types of T2w MS lesion images	Noise level					Execution time
	1%	3%	5%	7%	9%	
Noisy	39.8498	30.0116	25.4794	22.5058	20.3044	
	0.9353	0.7452	0.6223	0.5394	0.4790	
NL-PCA	44.0065	37.1081	34.1045	32.0699	30.4990	377
	0.9907	0.9583	0.9299	0.9011	0.8738	
PRI-NL-PCA	**44.3403**	**37.7557**	34.7161	32.6087	30.9775	468
	0.9925	0.9662	0.9445	0.9236	0.9006	
PNLM-PCA	44.3078	37.7550	**34.7699**	**32.7409**	**31.1667**	428
	0.9925	**0.9776**	**0.9646**	**0.9462**	**0.9190**	
Bw-NL-PCA	43.9639	37.2529	34.3705	32.4059	30.8968	605
	0.9901	0.9569	0.9301	0.9037	0.8787	
BM4D	43.7265	37.1584	34.4008	32.5827	31.1571	290
	0.9904	0.9618	0.9426	0.9230	0.8993	
PRI-Bh	43.6391	37.0868	34.1427	32.2287	30.7837	168
	0.9925	0.9727	0.9491	0.9340	0.9124	
PNLM-Bh	43.5847	36.9273	33.9865	32.0804	30.5898	123
	0.9925	0.9767	0.9580	0.9421	0.9182	

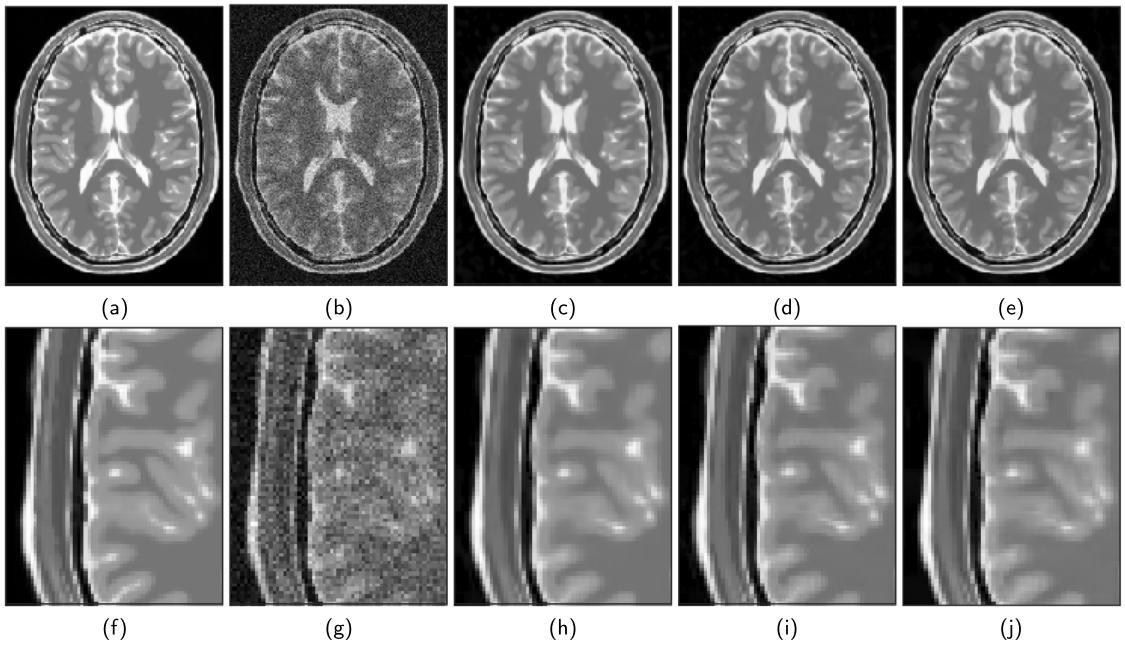

Fig. 1. One denoised T2w example from the BrainWeb dataset. (a) and (f) the noise-free image, (b) and (g) the noisy image, (c) and (h) PRI-NL-PCA, (d) and (i) PNLM-PCA, (e) and (j) BM4D.

The proposed PNLM-PCA method obtained the best results in most of the cases. The results obtained from different types of images are consistent.

3.4. Appraisal on clinical data

Actual MRI display systems usually have a 12- or 16-bit depth (4096 or 32768 gray levels observed) [26]. If the method of traversing values is used, the computational cost will be much greater than traversing coordinates. We naturally think of using scaling to compress the range of the image from 0 to 255. However, it should be noted that there are only a few high-value voxels in the magnetic resonance image [26]. When directly using the maximum value of the image for scaling, the noise level calculated is equal to σ_g divided by the maximum signal intensity of the image. The λ in the double restriction of formula (9) and (12) will be biased. The signal intensity of the overall image will be relatively low under this scaling. As mentioned earlier, the significance of λ is not only to accelerate but also to improve accuracy. A large number of other voxels in the formula (7) that are dissimilar to the voxel i are considered, and even small weights cannot suppress their contribution to the estimated signal intensity of voxel i. Therefore, we set a new ratio parameter for scaling:

$$rt = \frac{threshold}{255} \tag{16}$$

We can obtain the threshold through the distribution map of image signal intensity. The nonzero signal intensity distribution of a PDw normal image in BrainWeb is shown in Fig. 2.

Simulation data, which are simplifications of real images, may not accurately represent realistic details. So, this paper used two datasets to qualitatively test the consistency of the performance of PNLM-PCA on clinical data.

The first was a 3D MP-RAGE T1w volumetric sequence from the Human Connectome Project (HCP) database [27–30] acquired on a customized Siemens Skyra 3T scanner with TR=2400 ms, TE=2.14 ms, TI=1000 ms, flip angle=8°, voxel resolution=$0.7 \times 0.7 \times 0.7$ mm^3, and $260 \times 311 \times 260$ voxels [31]. From Fig. 2 we manually set threshold = 1024. The Rician noise level was estimated to be 1.02% of maximum intensity. Fig. 3 provides a comparison of filtering results on this dataset. No significant anatomical information exists in any residual images, indicating that the proposed methods successfully removed

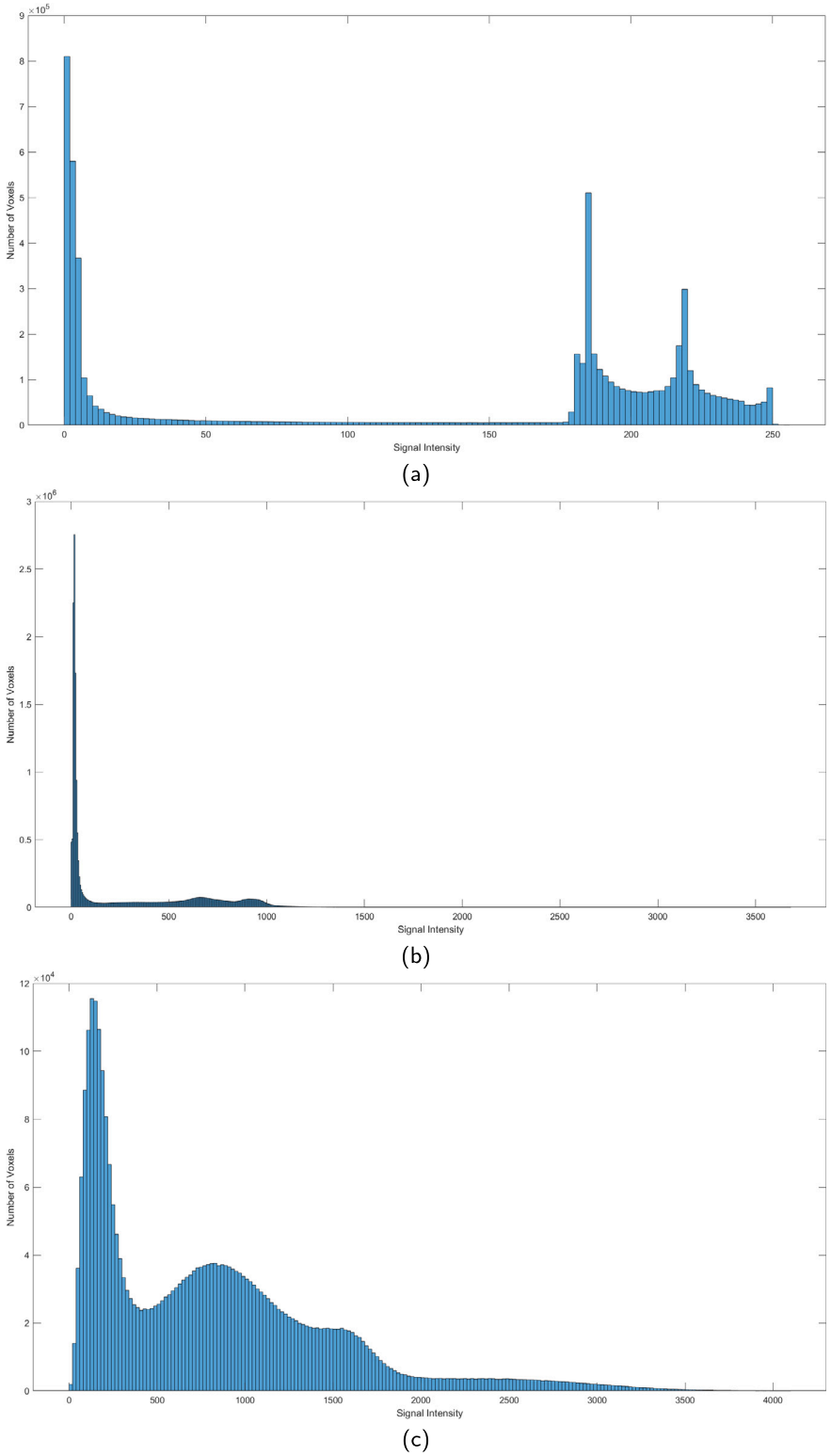

Fig. 2. The non-zero signal intensity distribution of three MR images. (a) a PDw normal image from the BrainWeb dataset. The maximum signal intensity of it is 255. (b) a T1w image from the HCP dataset. The maximum signal intensity of it is 3678. (c) a T1w image from the OASIS dataset. The maximum signal intensity of it is 4095.

noise. However, from the background of residual images, it can be seen that the PNLM-PCA technique demonstrates a slightly superior performance in noise removal when compared to PRI-NL-PCA. Both methods outperform BM4D. Excellent denoising performance will be beneficial for some fine anatomical details of the image to become clearer. This dataset took 1347 s to process with the PRI-NL-PCA filter, 1281 s with the PNLM-PCA filter, and 900 s with the BM4D.

The second was a magnetization prepared rapid gradient-echo (MP-RAGE) T1w volumetric sequence from the Open Access Series of Imaging Studies (OASIS) database acquired on a 1.5-T Vision scan-

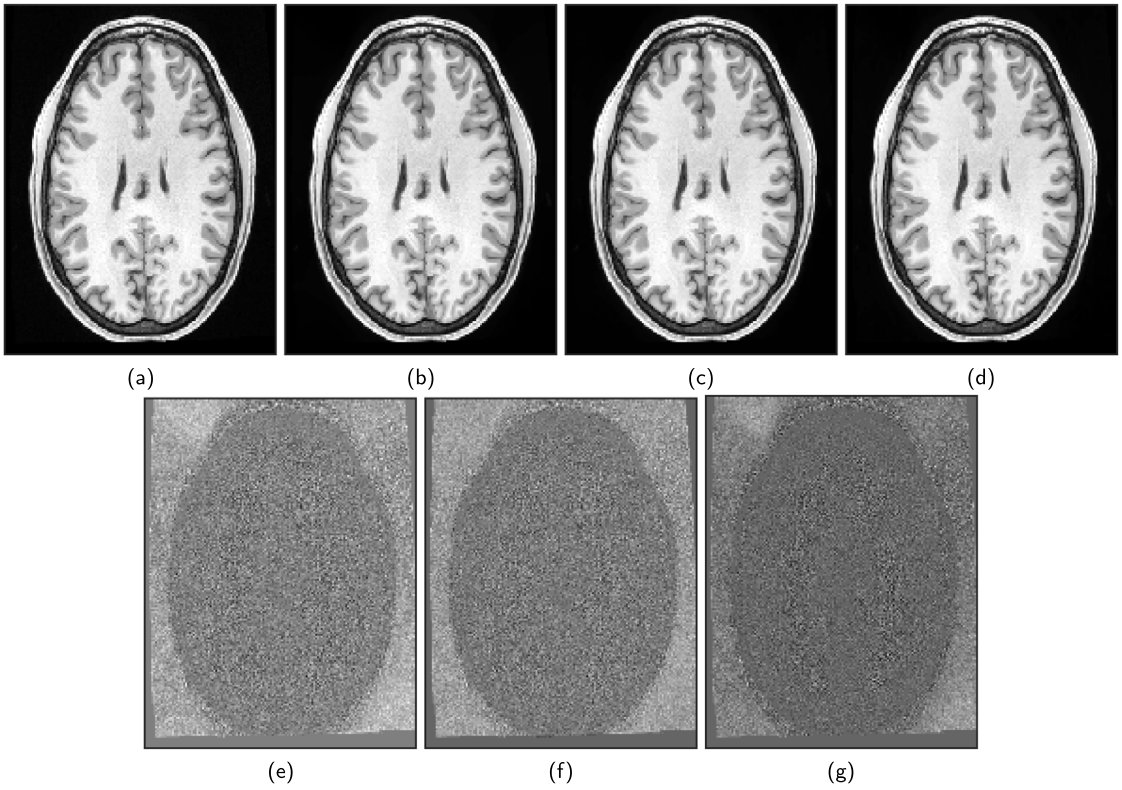

Fig. 3. One denoised T1w example from the HCP dataset. (a) the noisy image, (b) PRI-NL-PCA, (c) PNLM-PCA, (d) BM4D, (e) the residual map of (b), (f) the residual map of (c), (g) the residual map of (d).

Table 3
PSNR and SSIM measurement of different methods on PDw normal images with different noise levels.

Denoising types of PDw normal images	Noise level				
	1%	3%	5%	7%	9%
Noise	39.8418	30.0352	25.4813	22.5085	20.3211
	0.9293	0.7100	0.5656	0.4751	0.4154
NL-PCA	44.8669	38.3089	35.2346	33.2245	31.6864
	0.9899	0.9575	0.9266	0.8983	0.8770
PRI-NL-PCA	**45.3957**	38.9740	35.9376	33.8177	32.1947
	0.9919	0.9643	0.9422	0.9208	0.9022
PNLM-PCA	45.3500	**39.0249**	**36.0629**	**34.0558**	32.5400
	0.9917	**0.9767**	**0.9611**	**0.9418**	**0.9301**
Bw-NL-PCA	44.9489	38.5885	35.6284	33.6611	32.2136
	0.9895	0.9567	0.9269	0.9010	0.8830
BM4D	44.7536	38.5851	35.7992	33.9715	**32.5472**
	0.9897	0.9606	0.9395	0.9208	0.9025
PRI-Bh	44.7362	38.3902	35.4731	33.4499	31.8649
	0.9916	0.9658	0.9477	0.9278	0.9060
PNLM-Bh	44.5995	38.1214	35.2908	33.3400	31.7824
	0.9916	0.9585	0.9482	0.9355	0.9178

ner (Siemens, Erlangen, Germany) with TR=9.7 ms, TE=4.0 ms, TI=20 ms, TD=200 ms, flip angle=10°, voxel resolution= $1\times1\times1.25$ mm^3, and 256 × 256 × 128 voxels [32]. From Fig. 2 we set the threshold = 3072. The Rician noise level was estimated to be 3.15% of the maximum intensity. Fig. 4 shows the example results of filtering this dataset. It was noticed that all of these schemes performed very well on this dataset, but at the close-up, the BM4D and PRI-NL-PCA algorithms slightly over blurred the MR image, whereas the PNLM-PCA method effectively preserved fine details. The results reflect the excellent and robust performance of the PNLM-PCA algorithm. This dataset took 438 s to process with the PRI-NL-PCA filter, 550 s with the PNLM-PCA filter, and 361 s with the BM4D filter. The reason why PNLM-PCA ran slower than PRI-NL-PCA this time is likely due to the internal implementation of PNLM-PCA. If C_0 in formula (10) becomes the cube root of the product of size in three dimensions, it may be faster. However, simultaneously, the denominator may also require corresponding adjustment.

4. Discussion

This study found the optimal parameters of NL-PCA using particle swarm optimization. Additionally, we also propose the idea of traversing values instead of coordinates by utilizing the limited range and discrete properties of grayscale levels, and improve the PRI-NLM in PRI-NL-PCA. For the weight function, the square term of the local mean difference is omitted to improve the computational speed, and an additional constraint is added to improve the accuracy of the signal intensity estimation. Subsequently, based on mathematical principles, random uniform sampling is carried out to achieve speed improvement. This paper verifies the optimality of the NL-PCA scheme in Manjón et al. [11] and improves the objectivity of the selection of algorithm parameters. Contrary to the original literature, using a median filter when the noise level is not particularly high will reduce the noise reduction effect of the NL-PCA algorithm. In contrast to the findings reported by Manjón et al. [11], the results obtained using the suggested formula (2) exhibit a notable disparity compared to the direct input of the precise noise level. Only by adopting the latter method can we obtain the same good denoising results as Manjón et al. [11]. After improving the PRI-NLM part in PRI-NL-PCA, the final algorithm has higher PSNR, SSIM, and running speed than the original algorithm. From the experimental results in Jiang et al. [19] and Ran et al. [1], it can be inferred that, when only considering ROI, the PNLM-PCA denoising performance proposed in this paper can compete with deep learning algorithms. Although the speed may not necessarily be as fast as the pre-trained deep learning model, its universality will be better.

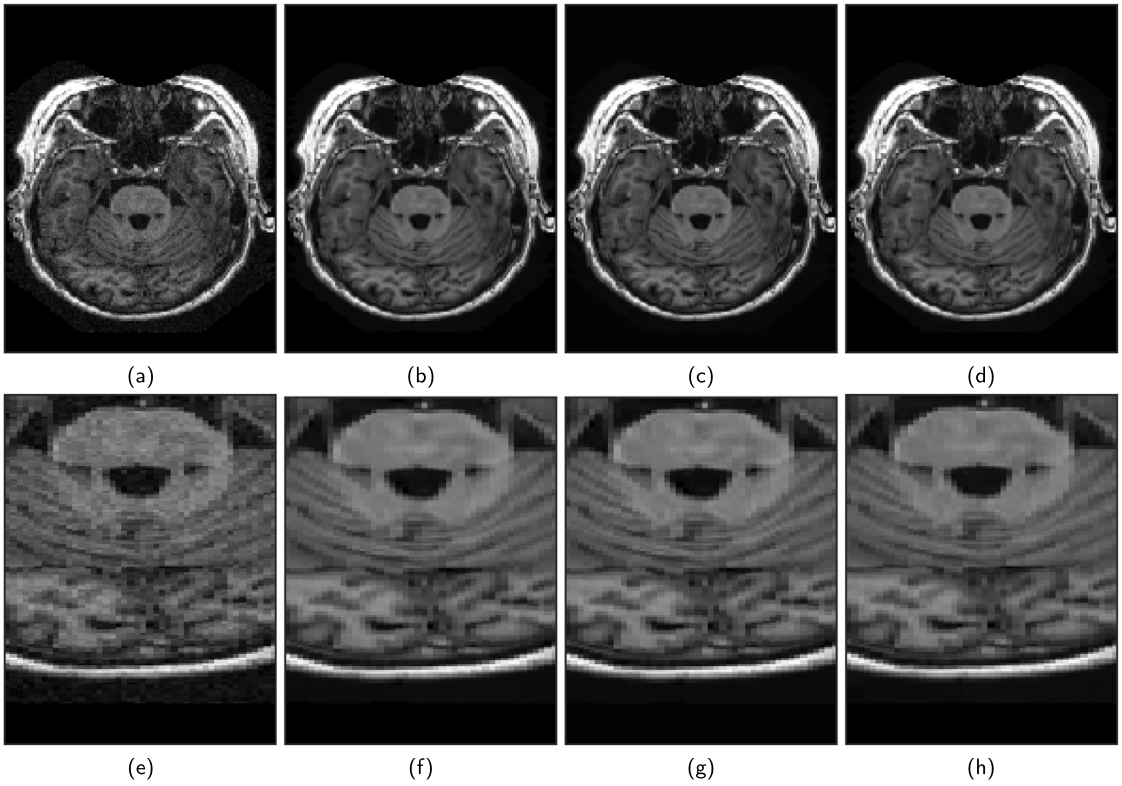

Fig. 4. One denoised T1w example from the OASIS dataset. (a) and (e) the noisy image, (b) and (f) PRI-NL-PCA, (c) and (g) PNLM-PCA, (d) and (h) BM4D.

Manjón and Coupe [33] also trained a CNN model, but its denoising effect was just comparable to PRI-NL-PCA.

The innovation of this article lies in the following points. First, we proposed the PNLM-PCA algorithm, which not only has better denoising performance than PRI-NL-PCA, but also has faster speed in most cases. When the internal estimator of PNLM-PCA adopts the formula (5), this algorithm is also expected to be used to remove Gaussian noise in natural images. Second, this article presents a novel structure of NLM. In previous work, NLM algorithms often had a filtering parameter related to the search window, and they did not fully achieve non-local in order to reduce computational cost. The search window of the proposed NLM is directly extended to the global level, fully considering all voxels in the entire image that are similar to a specific voxel in the image. At the same time, the computational cost of it is even lower than that of previous NLMs. The new NLM algorithm shares some common characteristics with most existing NLMs. The preservation of image edges may not be optimal when using fixed filtering parameters, such as the search window, patch size, and filtering coefficient. The λ of this work is also similar. To maximize the performance of PNLM-PCA, it is necessary to make it vary with noise variance. The structure proposed in this article is conducive to promoting the development of denoising algorithms based on NLM. Behind this new structure lies a computational method. For some univariate or multivariate functions, calculating all elements of the matrix simultaneously can be impractical, especially for matrices with enormous sizes, and traversing each element can be time-consuming to calculate. If the range of values for matrix elements is not very large, it can be calculated based on the distribution of values without the need to traverse all voxels.

This work still has several limitations that need to be solved in the future. First, when processing real clinical images, it is necessary to manually set thresholds based on the distribution of non-zero signal intensity for different images, and there is currently no standard for determining the optimal threshold. Second, the sg in the formula (10) requires correction. For instance, C_0 can be adjusted to the cube root of the product of the size of the three dimensions of the matrix, and the denominator may also need to be adjusted accordingly. Third, the running speed of PNLM-PCA is still not fast enough, mainly due to the PCA stage. To enhance efficiency, structure optimizations or alternative algorithms with comparable or superior results should be explored. Future work can also consider further optimizing the weight function w of the NLM algorithm.

Good traditional algorithms are not overly dependent on the object being denoised. They should not be eliminated and can still be utilized in the future. Furthermore, we are interested in investigating the potential applications of extending our proposed PNLM-PCA algorithm to deal with image noise in spines, livers, or knees.

CRediT authorship contribution statement

Shiao Li: Writing – review & editing, Writing – original draft, Visualization, Validation, Supervision, Software, Resources, Project administration, Methodology, Investigation, Funding acquisition, Formal analysis, Data curation, Conceptualization. **Fei Wang:** Writing – review & editing. **Song Gao:** Writing – review & editing.

Declaration of competing interest

None.

Acknowledgments

This work was supported by the National Natural Science Foundation of China (No. 12075011 and No. 62301010). Data were provided in part by OASIS-1: Cross-Sectional: Principal Investigators: D. Marcus, R, Buckner, J, Csernansky J. Morris; P50 AG05681, P01 AG03991, P01 AG026276, R01 AG021910, P20 MH071616, U24 RR021382. Data were also provided by the Human Connectome Project, WU-Minn Consortium (Principal Investigators: David Van Essen and Kamil Ugurbil; 1U54MH091657) funded by the 16 NIH Institutes and Centers that support the NIH Blueprint for Neuroscience Research; and by the McDonnell Center for Systems Neuroscience at Washington University.

References

[1] M. Ran, J. Hu, Y. Chen, H. Chen, H. Sun, J. Zhou, Y. Zhang, Denoising of 3D magnetic resonance images using a residual encoder–decoder Wasserstein generative adversarial network, Med. Image Anal. 55 (2019) 165–180.

[2] H.V. Bhujle, B.H. Vadavadagi, NLM based magnetic resonance image denoising – A review, Biomed. Signal Process. Control 47 (2019) 252–261.

[3] D. Muresan, T. Parks, Adaptive principal components and image denoising, in: Proceedings 2003 International Conference on Image Processing, Cat. No.03CH37429, Vol. 1, IEEE, Barcelona, Spain, 2003, pp. I–101–4.

[4] L. Zhang, W. Dong, D. Zhang, G. Shi, Two-stage image denoising by principal component analysis with local pixel grouping, Pattern Recognit. 43 (4) (2010) 1531–1549.

[5] L. Bao, M. Robini, W. Liu, Y. Zhu, Structure-adaptive sparse denoising for diffusion-tensor MRI, Med. Image Anal. 17 (4) (2013) 442–457.

[6] F. Lam, S.D. Babacan, J.P. Haldar, M.W. Weiner, N. Schuff, Z.-P. Liang, Denoising diffusion-weighted magnitude MR images using rank and edge constraints, Magn. Reson. Med. 71 (3) (2014) 1272–1284.

[7] A. Buades, B. Coll, J.M. Morel, A review of image denoising algorithms, with a new one, Multiscale Model. Simul. 4 (2) (2005) 490–530.

[8] J.V. Manjón, P. Coupé, A. Buades, V. Fonov, D. Louis Collins, M. Robles, Non-local MRI upsampling, Med. Image Anal. 14 (6) (2010) 784–792.

[9] P. Coupe, P. Yger, S. Prima, P. Hellier, C. Kervrann, C. Barillot, An optimized blockwise nonlocal means denoising filter for 3-D magnetic resonance images, IEEE Trans. Med. Imaging 27 (4) (2008) 425–441.

[10] J.V. Manjón, P. Coupé, A. Buades, D. Louis Collins, M. Robles, New methods for MRI denoising based on sparseness and self-similarity, Med. Image Anal. 16 (1) (2012) 18–27.

[11] J.V. Manjón, P. Coupé, A. Buades, MRI noise estimation and denoising using non-local PCA, Med. Image Anal. 22 (1) (2015) 35–47.

[12] S. Li, H. Chen, M. Wang, A.A. Heidari, S. Mirjalili, Slime mould algorithm: A new method for stochastic optimization, Future Gener. Comput. Syst. 111 (2020) 300–323.

[13] J. Tu, H. Chen, M. Wang, A.H. Gandomi, The colony predation algorithm, J. Bionic Eng. 18 (2021) 674–710.

[14] H. Su, D. Zhao, A.A. Heidari, L. Liu, X. Zhang, M. Mafarja, H. Chen, RIME: A physics-based optimization, Neurocomputing 532 (2023) 183–214.

[15] G.-G. Wang, S. Deb, Z. Cui, Monarch butterfly optimization, in: Neural Computing and Applications, Vol. 31, Springer, 2019, pp. 1995–2014.

[16] I. Ahmadianfar, A.A. Heidari, S. Noshadian, H. Chen, A.H. Gandomi, INFO: An efficient optimization algorithm based on weighted mean of vectors, Expert Syst. Appl. 195 (2022) 116516.

[17] A.A. Heidari, S. Mirjalili, H. Faris, I. Aljarah, M. Mafarja, H. Chen, Harris hawks optimization: Algorithm and applications, in: Future Generation Computer Systems, Vol. 97, Elsevier, 2019, pp. 849–872.

[18] J. Kennedy, R. Eberhart, Particle swarm optimization, in: Proceedings of ICNN'95 - International Conference on Neural Networks, Vol. 4, IEEE, Perth, WA, Australia, 1995, pp. 1942–1948.

[19] D. Jiang, W. Dou, L. Vosters, X. Xu, Y. Sun, T. Tan, Denoising of 3D magnetic resonance images with multi-channel residual learning of convolutional neural network, Jpn. J. Radiol. 36 (9) (2018) 566–574.

[20] C.G. Koay, P.J. Basser, Analytically exact correction scheme for signal extraction from noisy magnitude MR signals, J. Magn. Reson. 179 (2) (2006) 317–322.

[21] P. Coupé, J.V. Manjón, E. Gedamu, D. Arnold, M. Robles, D.L. Collins, An object-based method for Rician noise estimation in MR images, in: Medical Image Computing and Computer-Assisted Intervention–MICCAI 2009: 12th International Conference, London, UK, September 20-24, 2009, Proceedings, Part II. Vol. 12, Springer, 2009, pp. 601–608.

[22] D. Collins, A. Zijdenbos, V. Kollokian, J. Sled, N. Kabani, C. Holmes, A. Evans, Design and construction of a realistic digital brain phantom, IEEE Trans. Med. Imaging 17 (3) (1998) 463–468.

[23] R.-S. Kwan, A. Evans, G. Pike, MRI simulation-based evaluation of image-processing and classification methods, IEEE Trans. Med. Imaging 18 (11) (1999) 1085–1097.

[24] Z. Wang, A.C. Bovik, H.R. Sheikh, E.P. Simoncelli, Image quality assessment: from error visibility to structural similarity, IEEE Trans. Image Process. 13 (4) (2004) 600–612.

[25] M. Maggioni, V. Katkovnik, K. Egiazarian, A. Foi, Nonlocal transform-domain filter for volumetric data denoising and reconstruction, IEEE Trans. Image Process. 22 (1) (2013) 119–133.

[26] D.W. McRobbie, E.A. Moore, M.J. Graves, M.R. Prince, MRI from Picture to Proton, Cambridge University Press, 2017.

[27] M.F. Glasser, S.N. Sotiropoulos, J.A. Wilson, T.S. Coalson, B. Fischl, J.L. Andersson, J. Xu, S. Jbabdi, M. Webster, J.R. Polimeni, D.C. Van Essen, M. Jenkinson, The minimal preprocessing pipelines for the Human Connectome Project, NeuroImage 80 (2013) 105–124, Mapping the Connectome.

[28] M. Jenkinson, C.F. Beckmann, T.E. Behrens, M.W. Woolrich, S.M. Smith, FSL, NeuroImage 62 (2) (2012) 782–790, 20 YEARS OF fMRI.

[29] B. Fischl, FreeSurfer, NeuroImage 62 (2) (2012) 774–781, 20 YEARS OF fMRI.

[30] M. Jenkinson, P. Bannister, M. Brady, S. Smith, Improved optimization for the robust and accurate linear registration and motion correction of brain images, NeuroImage 17 (2) (2002) 825–841.

[31] J.S. Elam, M.F. Glasser, M.P. Harms, S.N. Sotiropoulos, J.L. Andersson, G.C. Burgess, S.W. Curtiss, R. Oostenveld, L.J. Larson-Prior, J.-M. Schoffelen, et al., The human connectome project: a retrospective, NeuroImage 244 (2021) 118543.

[32] D.S. Marcus, T.H. Wang, J. Parker, J.G. Csernansky, J.C. Morris, R.L. Buckner, Open Access Series of Imaging Studies (OASIS): cross-sectional MRI data in young, middle aged, nondemented, and demented older adults, J. Cogn. Neurosci. 19 (9) (2007) 1498–1507.

[33] J.V. Manjón, P. Coupe, MRI denoising using deep learning and non-local averaging, 2019, arXiv preprint arXiv:1911.04798.